Crystal and magnetic structure of Cr- and Ni-substituted $(La_{0.50}Ca_{0.50})MnO_3$

2008 J. Phys.: Condens. Matter 20 145210

(http://iopscience.iop.org/0953-8984/20/14/145210)

J. Phys.: Condens. Matter **20** (2008) 145210 (10pp) doi:10.1088/0953-8984/20/14/145210

Crystal and magnetic structure of Cr- and Ni-substituted $(La_{0.50}Ca_{0.50})MnO_3$

A Martinelli[1,5], M Ferretti[1,2], C Castellano[1], M R Cimberle[3] and C Ritter[4]

[1] Laboratory of Innovative and Artificial Materials, INFM-CNR, Corso Perrone 24, 16152 Genova, Italy
[2] Department of Chemistry and Industrial Chemistry, University of Genvoa, Via Dodecaneso 31, 16146 Genova, Italy
[3] Istituto dei Materiali per l'Elettronica ed il Magnetismo, National Research Council, c/o Department of Physics, University of Genova, Via Dodecaneso 33, 16146, Genova, Italy
[4] Institute Laue-Langevin, 6 rue Jules Horowitz, 38042 Grenoble Cedex 9, France

E-mail: amartin@chimica.unige.it

Received 17 January 2008, in final form 21 February 2008
Published 19 March 2008
Online at stacks.iop.org/JPhysCM/20/145210

Abstract

The crystal and magnetic structure of $(La_{0.50}Ca_{0.50})(Mn_{1-x}B_x)O_3$ ($x = 0.00, 0.03, 0.08$; B = Cr, Ni) has been investigated between 5 and 300 K by means of dc magnetic measurements and neutron powder diffraction followed by Rietveld refinement. In the pristine compound an orthorhombic to monoclinic phase transition is detected on cooling, accompanied by a CE-type antiferromagnetic (AFM) ordering arising. Ni^{2+} and Cr^{3+} substitutions have similar effects on the structural and magnetic properties of $(La_{0.50}Ca_{0.50})MnO_3$, despite the fact that these ions are characterized by different external electronic configurations. After substitution, the orthorhombic to monoclinic phase transition is hindered. As a consequence, charge and orbital orderings are suppressed, as is the superexchange; double exchange takes place inducing ferromagnetic (FM) interactions. No evidence for stable magnetic interaction between Cr^{3+} or Ni^{2+} and the neighbouring Mn ions was detected. Nevertheless, in the Ni-substituted samples a detectable quantity of monoclinic phase forms during cooling, inside which AFM interactions take place. The amount of this secondary monoclinic phase decreases on increasing Ni substitution; the global FM magnetic moment decreases as well, due to a spin-cluster glass-type state arising. As a result a FM state is found to coexist with a spin-cluster glass-type state.

(Some figures in this article are in colour only in the electronic version)

1. Introduction

The class of compounds referred to as rare earth manganites is characterized by extremely interesting structural and physical properties; depending on composition, the ordering of the Mn^{3+} and Mn^{4+} cationic species can take place in the Mn sublattice (charge ordering: CO), that can be coupled with the ordering of the Mn^{3+} e_g orbitals (orbital ordering: OO). From a physical point of view, different compositions can favour or hinder ferromagnetic (FM) or antiferromagnetic (AFM) spin ordering in the Mn sublattice, as well as colossal magnetoresistance (CMR) [1]. As a consequence the substitution at the Mn site with different atomic species can strongly control both structural and physical properties. In particular $(La_{0.50}Ca_{0.50})MnO_3$ represents a boundary between competing FM and CO-AFM ground state, a favourable scenario for phase separation phenomena [2]; hence by means of an appropriate substitution at the Mn site it is possible to favour one of the competing phases.

Phase coexistence in $(La_{0.50}Ca_{0.50})MnO_3$ was directly observed by means of transmission electron microscopy (TEM) below 240 K [3]. A subsequent TEM investigation ascertained that the FM state is characterized by the fine coexistence of an AFM incommensurate CO phase with a FM charge disordered one [4]; as the T was decreased the system is eventually constituted of an AFM CO–OO phase. This

[5] Author to whom any correspondence should be addressed.

study highlighted the need to discriminate between CO and OO, since CO with incommensurate OO occurs in the FM phase [4]; at the FM to AFM transition an incommensurate to commensurate OO takes place. The structural refinement of the CO–OO monoclinic phase revealed a quasi-commensurate OO, whereas CO was found long range commensurate and coupled with the magnetic ordering; the presence of a small amount of untransformed orthorhombic phase at low T was detected as well and was related to a small AFM reflection arising [5]. A subsequent investigation ascertained the FM character of this secondary phase that discontinuously transforms into the AFM one as a function of T or magnetic field [6]. Noteworthy phase separation can be controlled by the microstructural properties of the samples: in particular the FM fraction at low T was found to increase with the decrease of the average grain size [7, 8].

It is well known that both Ni^{2+} and Cr^{3+} suppress CO and OO in half doped manganites [9, 10] and induce a FM metallic state under zero magnetic field; this fact has been ascribed to the possibility of these cationic species to exhibit itinerant electrons in oxides with high valence state that possibly participate in the double exchange [9–11]. Conversely other investigations state a superexchange interaction between Cr^{3+} and Mn^{3+} [12–14], although some authors suggest a FM spin alignment, whereas others propose that Cr^{3+} substitutes Mn^{3+} with opposite spin. Whatever the case, the ordering of the magnetic moments of both Ni^{2+} and Cr^{3+} in the manganite implies the participation of these ions to double or superexchange.

Despite the large number of studies evidencing the primary role of Ni^{2+} and Cr^{3+} in determining the magnetic properties of these compounds, accurate investigations concerning the structural effects of Ni^{2+} and Cr^{3+} in $(La_{0.50}Ca_{0.50})MnO_3$ are lacking. In order to favour the FM component of this intrinsically phase separated compound, we carried out Ni and Cr substitution at the Mn site and studied the structural evolution of Ni- and Cr-substituted $(La_{0.50}Ca_{0.50})MnO_3$ as a function of temperature, investigating how structural changes can affect the magnetic properties as well.

2. Experimental details

Polycrystalline $(La_{0.50}Ca_{0.50})(Mn_{1-x}B_x)O_3$ samples with B = Ni, Cr and x = 0.00, 0.03, 0.08 were prepared by means of a solid state reaction: binary oxides (CaO 99.95% ALDRICH; La_2O_3 99.99% ALFA AESAR; MnO_2 99.999% ALFA AESAR, Cr_2O_3 99.997% ALFA AESAR; NiO 99.998% ALFA AESAR;) were firstly sieved (80 mesh), then mixed in stoichiometric amounts and finally reacted at high temperature in air. Four thermal treatments with intermediate grinding were carried out, the first at 1523 K for 15 h and the remaining at 1603 K for 18 h. X-ray powder diffraction analysis (PHILIPS PW1830; Bragg–Brentano geometry; Cu Kα; secondary monochromator; 2θ range: 13°–80°; step: 0.02° 2θ; sampling time: 15 s) did not evidence the presence of secondary phases. The samples were characterized by magnetic measurements using a Quantum Design SQUID magnetometer. The minimum in the first derivative of the FC curve were assumed as the Curie temperature (T_C); saturation magnetization (M_s) was obtained by magnetization curves collected at 5 K up to 5.5 T. Neutron powder diffraction (NPD) analysis was carried out at the Institute Laue-Langevin using the D1A diffractometer; diffraction patterns were collected between 10 and 300 K using a wavelength of $\lambda = 1.91$ Å. The crystal and magnetic structures were refined using the program FULLPROF [15].

In the following, referring to the samples, also the ABO_3 formula is used (A: La, Ca; B: Mn, Cr, Ni).

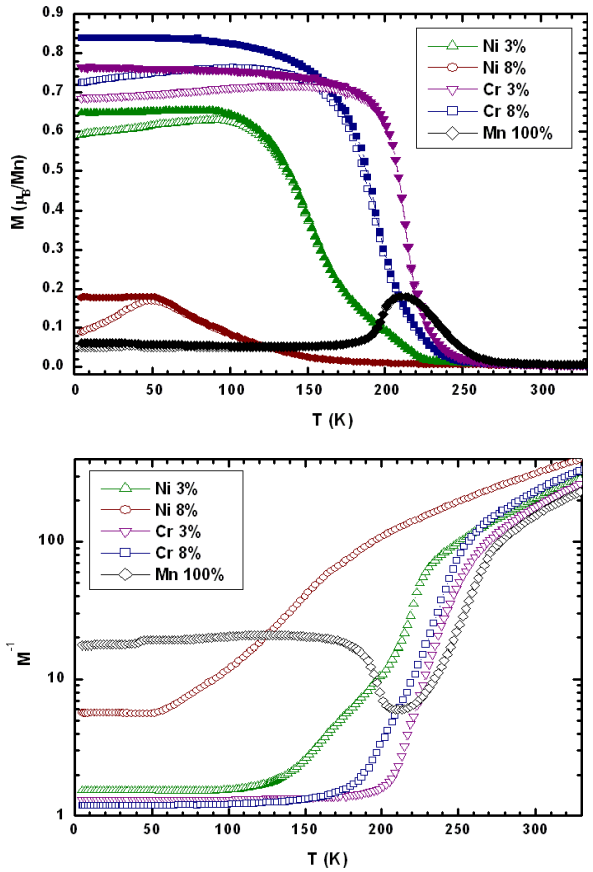

Figure 1. Upper panel: Comparison of FC (closed symbols), ZFC (open symbols) dc magnetization versus T curves for both pristine and substituted samples. Lower panel: inverse magnetization (logarithmic scale) as a function of T.

3. Results and discussion

3.1. $(La_{0.50}Ca_{0.50})MnO_3$

Both structural and physical properties of this compound have been extensively investigated in previous works; hence, in this section we present only the main results obtained that are used as a starting point for the discussion in the following sections concerning Cr and Ni substitution.

The sample exhibits the classical magnetic behaviour characterizing the $(La_{0.50}Ca_{0.50})MnO_3$ composition. Figures 1 and 2 show the dependence of ZFC and FC dc magnetization as a function of T at $\mu_0 \cdot H = 5 \times 10^{-2}$ T and the magnetization

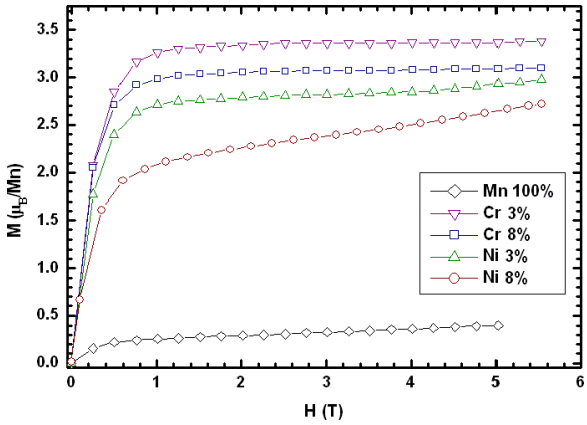

Figure 2. Magnetization versus field at 5 K as a function of substitution at the Mn site in $(La_{0.50}Ca_{0.50})MnO_3$.

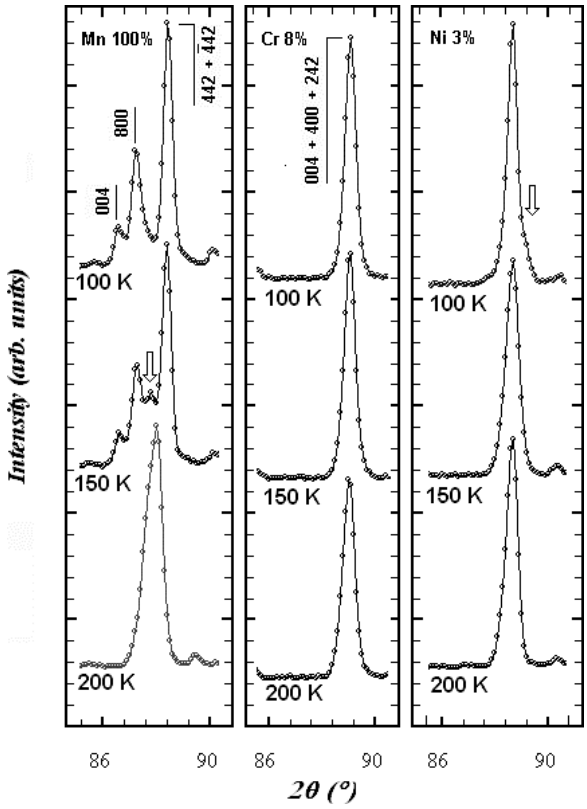

Figure 3. Selected portions of NPD patterns ($\lambda = 1.91$ Å) collected around the orthorhombic to monoclinic structural transition; the indexing of the monoclinic and orthorhombic peaks is shown in the left and the central panel, respectively. Left panel: phase coexistence at 150 K in $(La_{0.50}Ca_{0.50})MnO_3$: the arrow evidences the orthorhombic nuclear peak that progressively vanishes on cooling. Central panel: NPD patterns of $(La_{0.50}Ca_{0.50})(Mn_{0.92}Cr_{0.08})O_3$ where no evidence of phase coexistence or line broadening can be detected. Right panel: anisotropic line broadening towards high angle (arrowed) in $(La_{0.50}Ca_{0.50})(Mn_{0.97}Ni_{0.03})O_3$ patterns originated by the occurrence of the secondary monoclinic phase.

versus magnetic field at 5 K, respectively. At 300 K the sample is paramagnetic (PM) and upon cooling it first exhibits FM ($T_C \sim 231$ K) and then becomes AFM ($T_N \sim 160$ K).

NPD patterns collected on our sample are characterized by a small angle neutron scattering (SANS) contribution above

Table 1. Selected structural parameters and R factors for $(La_{0.50}Ca_{0.50})MnO_3$ obtained after Rietveld refinement of NPD data collected at 10 K (space group: $P2_1/m$).

a (Å)		10.8803(4)		
b (Å)		7.5166(2)		
c (Å)		5.4703(2)		
β (deg)		90.0896(5)		
Atom	Site	x	y	z
A1(La, Ca)	2e	0.0077(1)	1/4	0.0053(4)
A2(La, Ca)	2e	0.2417(2)	1/4	0.5004(3)
A3(La, Ca)	2e	0.2589(2)	1/4	0.5123(3)
A4(La, Ca)	2e	0.4852(1)	1/4	0.0070(3)
Mn^{4+}	4f	0.2499(2)	0.0065(2)	0.0052(2)
Mn^{3+}	2c	0	0	1/2
Mn^{3+}	2d	1/2	0	1/2
$O_{ax}1$	2e	0.5030(1)	1/4	0.4265(3)
$O_{ax}2$	2e	0.2643(2)	1/4	0.9543(3)
$O_{ax}3$	2e	0.2418(2)	1/4	0.0740(3)
$O_{ax}4$	2e	0.9978(1)	1/4	0.5599(4)
$O_{eq}1$	4f	0.3586(1)	0.5426(2)	0.2979(2)
$O_{eq}2$	4f	0.3831(1)	0.4721(2)	0.7893(2)
$O_{eq}3$	4f	0.1135(1)	0.9594(2)	0.2433(2)
$O_{eq}4$	4f	0.1370(1)	0.0275(2)	0.7492(2)
R_{Bragg} (%)	R_F (%)	$R_{magnetic}$ Mn^{3+} (%)		$R_{magnetic}$ Mn^{4+} (%)
4.52	4.25	9.11		14.3

the AFM transition which abruptly decreases between 200 and 150 K; below T_N scattering progressively decreases with cooling.

The crystal structure can be successfully refined in the orthorhombic $Pnma$ space group for $T > 150$ K; a closer analysis of the NPD data evidences a faint FM contribution in the pattern collected at 200 K. Selective splitting of diffraction lines takes place at $T \leqslant 150$ K, signing the occurrence of the CO–OO monoclinic phase and the suppression of FM. Hence using the structural data obtained applying the $Pnma$ structural model as a starting point, a new structural model in the $P2_1/m$ space group with the doubling of the a cell edge was obtained [5] and applied for the refinement of the data collected at $T \leqslant 150$ K. At 150 K phase coexistence was detected, as reported in figure 3 (left panel) where selected portions of the NPD patterns collected around the structural transition are shown, evidencing the progressive disappearance of the orthorhombic peak (arrowed) on cooling. At lower T the contribution of the orthorhombic phase to the NPD pattern, if present, is negligible.

With our experimental conditions it was not possible to ascertain the modulation wavevector of the superstructure, as detected by a previous synchrotron powder diffraction investigation, but, as a whole, the refined data are in good agreement with those reported [5]. The comparison of the R_{Bragg} and R_F factors confirms the higher reliability of the monoclinic structural model over the orthorhombic one at 10 K ($Pnma$: $R_{Bragg} = 6.46\%$; $R_F = 5.88\%$; $P2_1/m$: $R_{Bragg} = 4.52\%$; $R_F = 4.25\%$). The refined structural data obtained from the NPD data collected at 10 K are reported in table 1 and the corresponding Rietveld refinement plot in figure 4 (table 2 shows structural data at 300 K).

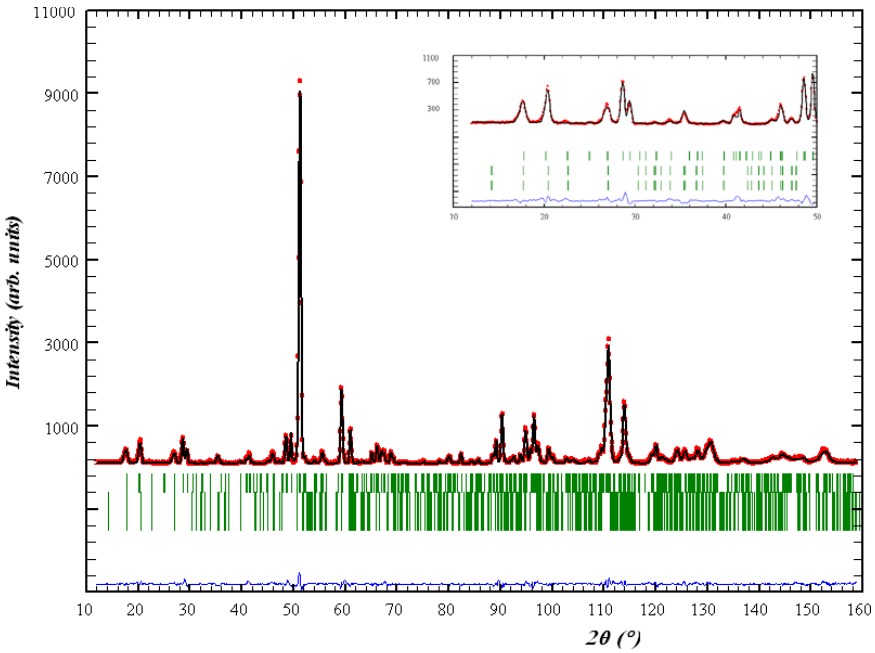

Figure 4. Rietveld refinement plot for $(La_{0.50}Ca_{0.50})MnO_3$ at 10 K; the inset is an enlarged view in the low 2θ region. The points in the upper field represent the observed intensity data, the calculated pattern is superposed and drawn as a solid line; the small vertical bars indicate the position of the allowed Bragg reflections for the nuclear phase (upper) and the two magnetic sublattices (middle: Mn^{3+} sublattice; lower: Mn^{4+} sublattice); the difference between the observed and calculated patterns is plotted in the lower field.

Table 2. Selected structural parameters and *R* factors for $(La_{0.50}Ca_{0.50})(Mn, B)O_3$ obtained after Rietveld refinement of NPD data collected at 300 K (space group: *Pnma*; Mn at 4b site).

		B = 0	B = Cr 3%	B = Cr 8%	B = Ni 3%	B = Ni 8%
a (Å)		5.4189(1)	5.4197(1)	5.4157(2)	5.4098(2)	5.4033(1)
b (Å)		7.6412(2)	7.6441(2)	7.6399(2)	7.6299(2)	7.6256(2)
c (Å)		5.4297(2)	5.4311(1)	5.4268(3)	5.4217(2)	5.4168(1)
V (Å^3)		224.83(1)	225.00(1)	224.54(2)	223.79(1)	223.19(1)
A(La, Ca)	*x*	0.0189(3)	0.0192(3)	0.0192(4)	0.0185(4)	0.0190(4)
	z	0.9960(5)	0.9955(5)	0.9960(6)	0.9962(5)	0.9965(5)
O_{ax}	*x*	0.9913(5)	0.9916(5)	0.9918(6)	0.9914(5)	0.9922(5)
	z	0.4409(4)	0.4408(4)	0.4405(5)	0.4414(4)	0.4414(4)
O_{eq}	*x*	0.7223(3)	0.7227(3)	0.7231(4)	0.7227(3)	0.7230(3)
	y	0.9687(1)	0.9688(1)	0.9687(2)	0.9684(2)	0.9687(2)
	z	0.2759(3)	0.2760(3)	0.2761(4)	0.2759(3)	0.2757(3)
Rf (%)		3.88	3.46	2.95	3.59	2.63
R_{Bragg} (%)		4.06	3.70	3.26	3.93	2.98
Mn–O_{ax} (Å)		1.9377(4)	1.9384(4)	1.9376(5)	1.9377(4)	1.9331(4)
Mn–O_{eq} (Å)		1.950(2)	1.948(2)	1.945(2)	1.950(2)	1.942(2)
Mn–O_{eq} (Å)		1.937(2)	1.939(2)	1.940(2)	1.937(2)	1.934(2)

The structural transition is accompanied by an AFM spin ordering arising, revealed by the occurrence of magnetic reflections in the NPD patterns collected at $T \leqslant 150$ K. It is well known that for $(La_{0.50}Ca_{0.50})MnO_3$ a *CE*-type spin ordering takes place at T_N [16]. By means of the representation analysis of magnetic structures [17] the consistency of this kind of spin ordering with the nuclear structure was checked. The magnetic Mn atoms are located at three different sites; Mn^{3+} is hosted at 2c and 2d sites with propagation vector $\mathbf{k} = (0, 0, 1/2)$, whereas Mn^{4+} at 4f with $\mathbf{k} = (0, 0, 1/2)$ (propagation vectors are indexed according to the monoclinic structure). The irreducible representations of the allowed magnetic structures were hence calculated and then the agreement between the observed and calculated diffraction patterns was checked. This analysis confirms that the Mn^{4+} and Mn^{3+} magnetic sublattices obey to different representations since the magnetic components along the *x* and *z* axes are arranged according to a *G*-type spin ordering for Mn^{4+} and to a *C*-type one for Mn^{3+}. The final result is consistent with the *CE*-type spin ordering as a whole [16]. The *x* and *z* components of the magnetic moment were refined independently for both magnetic sublattices. As a result the magnetic moments of both magnetic sublattices lie in the *ac* plane and their magnitudes are $\mu_{Mn^{3+}} = 2.76(4)\ \mu_B$ and $\mu_{Mn^{4+}} = 2.48(3)\ \mu_B$, quite below the theoretical spin-only values (4 μ_B

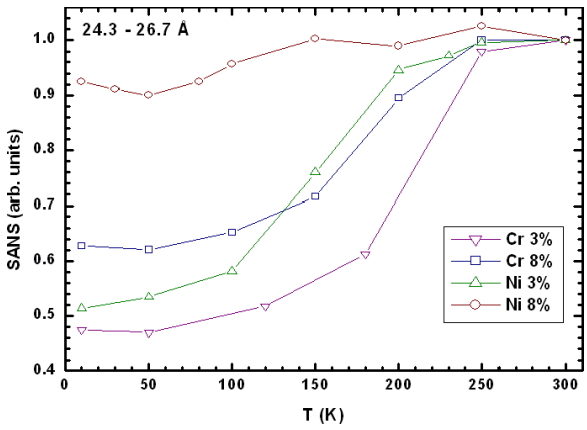

Figure 5. Evolution of SANS intensity as a function of T for the four substituted samples. In order to compare the behaviour of the different samples each point in the graph was calculated averaging the SANS intensity in the range 24.3–26.7 Å and then normalizing it to the value obtained at 300 K.

and 3 μ_B, respectively), but in good agreement with those reported for the *CE*-type structure in $(Pr_{0.50}Ca_{0.50})MnO_3$ [18], $(Nd_{0.50}Ca_{0.50})MnO_3$ [19], $(La_{0.50}Ca_{0.50})MnO_3$ [20].

3.2. Cr substitution

Assuming a stoichiometric O content in the examined samples, charge balance imposes a progressive decrease of Mn^{3+} as the Cr^{3+} substitution increases (for $x = 0.03$: $[Mn^{3+}]/[Mn^{4+}] = 0.94$; for $x = 0.08$: $[Mn^{3+}]/[Mn^{4+}] = 0.84$). As a consequence the theoretical spin-only values for FM saturation of the Mn lattice are 3.38 μ_B and 3.18 μ_B for $x = 0.03$ and 0.08, respectively.

ZFC–FC magnetization curves of both samples (figure 1) exhibit a typical FM behaviour with a sudden magnetization increase at T_C and a flat behaviour up to the lowest temperature. By increasing the Cr substitution the magnetic transition broadens and T_C decreases (for $x = 0.03$: $T_C \sim 211$ K; for $x = 0.08$: $T_C \sim 194$ K). For these samples M_s are respectively equal to 3.33 μ_B ($x = 0.03$) and 3.04 μ_B ($x = 0.08$), indicating a progressive faint decrease of the FM fraction with substitution. This result suggests that the magnetic moments of Cr^{3+} are not long range ordered within the Mn magnetic lattice. In fact in the case of FM coupling among Cr^{3+} and Mn cations the theoretical spin-only values of the B lattice are quite similar for both substitutions, 3.47 μ_B and 3.42 μ_B for $x = 0.03$ and 0.08, respectively; this result disagrees with the experimental one from both the quantitatively and qualitatively point of view. Conversely, for a pure AFM coupling the expected theoretical spin-only values (3.29 μ_B and 2.94 μ_B, respectively) are slightly lower than the experimental ones.

The NPD patterns of both samples exhibit SANS above T_C, that is abruptly suppressed as the magnetic structure arises (figure 5). This behaviour was already observed in Cr-substituted $(Pr_{0.55}Ca_{0.45})MnO_3$ samples [21] and is related to the development of FM clusters in the PM region, resulting in a strong contribution to SANS [22].

Below the magnetic transition FM peaks are observed, whereas the orthorhombic structure is retained during cooling. This fact indicates that Cr^{3+} substitution suppresses the orthorhombic to monoclinic transition and as a consequence the charge and orbital orderings are hindered. No evidence for a possible secondary monoclinic phase can be detected (figure 3, central panel). Figure 6 shows the Rietveld refinement plot obtained using the NPD data collected at

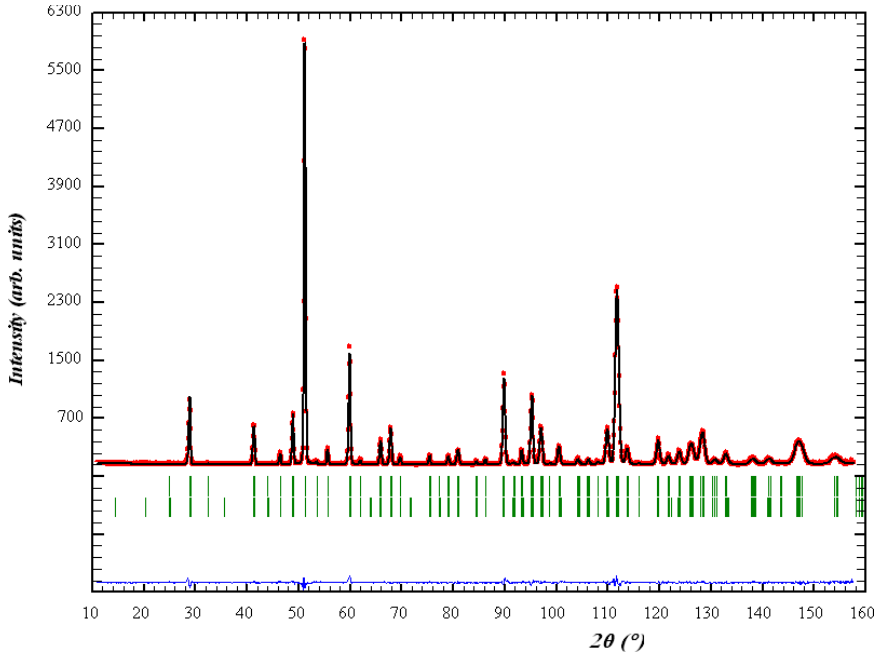

Figure 6. Rietveld refinement plot for $(La_{0.50}Ca_{0.50})(Mn_{0.92}Cr_{0.08})O_3$ (data collected at 10 K). The points in the upper field represent the observed intensity data, the calculated pattern is superposed and drawn as a solid line; the small vertical bars indicate the position of the allowed Bragg reflections for the nuclear phase (upper) and the FM magnetic one (lower); the difference between the observed and calculated patterns is plotted in the lower field.

Table 3. Selected structural parameters and R factors for $(La_{0.50}Ca_{0.50})(Mn, B)O_3$ obtained after Rietveld refinement of NPD data collected at 10 K (space group: *Pnma*: Mn at 4b site).

		B = Cr 3%	B = Cr 8%	B = Ni 3%	B = Ni 8%
a (Å)		5.4125(1)	5.4087(2)	5.4044(2)	5.4010(2)
b (Å)		7.6372(1)	7.6323(2)	7.6253(2)	7.6058(2)
c (Å)		5.4201(1)	5.4162(2)	5.4122(2)	5.4109(2)
V (Å^3)		224.05(1)	223.58(1)	223.04(1)	222.27(1)
A(La, Ca)	x	0.0218(3)	0.0217(3)	0.0214(5)	0.0221(4)
	z	0.9947(4)	0.9949(6)	0.9961(8)	0.9945(5)
O_{ax}	x	0.9920(4)	0.9912(5)	0.9916(7)	0.9919(5)
	z	0.4394(4)	0.4395(5)	0.4408(6)	0.4387(4)
O_{eq}	x	0.7230(3)	0.7225(4)	0.7228(5)	0.7221(4)
	y	0.9679(1)	0.9681(2)	0.9672(2)	0.9681(2)
	z	0.2769(3)	0.2764(4)	0.2770(5)	0.2764(4)
μ_B		3.09(2)	2.73(2)	2.96(3)	1.12(4)
Rf (%)		2.02	1.83	2.24	2.70
R_{Bragg} (%)		2.57	2.59	2.89	3.38
$R_{Magnetic}$ (%)		2.58	1.47	2.14	5.28
Mn–O_{ax} (Å)		1.9378(4)	1.9366(5)	1.9335(5)	1.9306(4)
Mn–O_{eq} (Å)		1.942(2)	1.944(2)	1.940(3)	1.943(2)
Mn–O_{eq} (Å)		1.941(2)	1.936(2)	1.939(3)	1.932(2)

10 K for the $(La_{0.50}Ca_{0.50})(Mn_{0.92}Cr_{0.08})O_3$ sample; structural data and agreement factors are reported in table 2 (300 K data) and table 3 (10 K data). For both samples the a and c cell edges homogeneously decrease with T (figure 7), whereas the behaviour of b is a little bit complicated. In $(La_{0.50}Ca_{0.50})(Mn_{0.97}Cr_{0.03})O_3$ a sudden decrease of b is detected at 250 K, but further cooling does not greatly change this value; in $(La_{0.50}Ca_{0.50})(Mn_{0.92}Cr_{0.08})O_3$ the value of b homogeneously decreases up to 200 K, but then a slight increase is observed up to a constant value.

Several magnetic structural models were tested in order to ascertain if the spins of Cr^{3+} are somehow aligned with those of the Mn ions or not. The best result in terms of *R-magnetic* factor was obtained with the structural model foreseeing the FM alignment of the Mn magnetic moments only and a random orientation of the Cr^{3+} spins, in agreement with the magnetization measurements. This result suggests that double or superexchange interactions do not occur between Cr^{3+} and the neighbouring Mn ions, but it is not definitive per se; in fact very small differences in the *R-magnetic* factors might appear due to the different magnetic form factors used for Cr^{3+} and Mn^{3+} but our data are not useful to study form factors differences. In any case the obtained result is in agreement with the magnetic measurements, indicating that the magnetic moments of Cr^{3+} are not long range ordered within the Mn magnetic lattice. The magnetic moments are aligned parallel to the c axis with 3.09(2) μ_B and 2.73(2) μ_B for $x = 0.03$ and 0.08, respectively; from the comparison of the theoretical spin-only values for FM saturation of the Mn lattice with these data it can be argued that at zero field ∼91% of the Mn moments are FM aligned in $(La_{0.50}Ca_{0.50})(Mn_{0.97}Cr_{0.03})O_3$, whereas this percentage decreases in $(La_{0.50}Ca_{0.50})(Mn_{0.92}Cr_{0.08})O_3$, being ∼86%. The remaining fraction of Mn moments is in a disordered arrangement. This result qualitatively agrees with the magnetization measurements carried out in a high-magnetic field where a progressive decrease of the FM fraction with Cr substitution is detected.

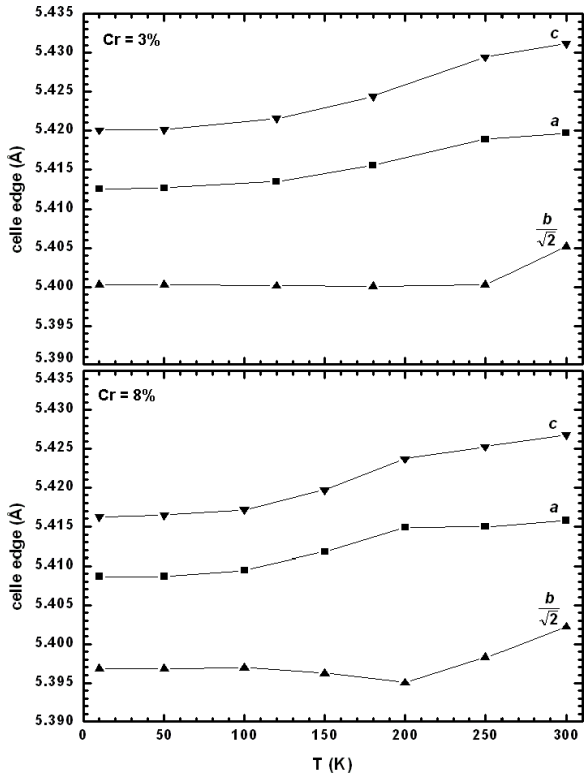

Figure 7. Evolution of the cell parameters as a function of T for $(La_{0.50}Ca_{0.50})(Mn_{0.97}Cr_{0.03})O_3$ and $(La_{0.50}Ca_{0.50})(Mn_{0.92}Cr_{0.08})O_3$; error bars are smaller than the symbols.

3.3. Ni substitution

The substitution at the Mn site with Ni^{2+} increases the hole doping (for $x = 0.03$: $[Mn^{3+}]/[Mn^{4+}] = 0.83$; for $x = 0.08$: $[Mn^{3+}]/[Mn^{4+}] = 0.59$) and the theoretical spin-only values for FM saturation of Mn cationic species are 3.35 μ_B and 3.10 μ_B for $x = 0.03$ and 0.08, respectively. It is interesting to observe that these values are quite similar to those calculated

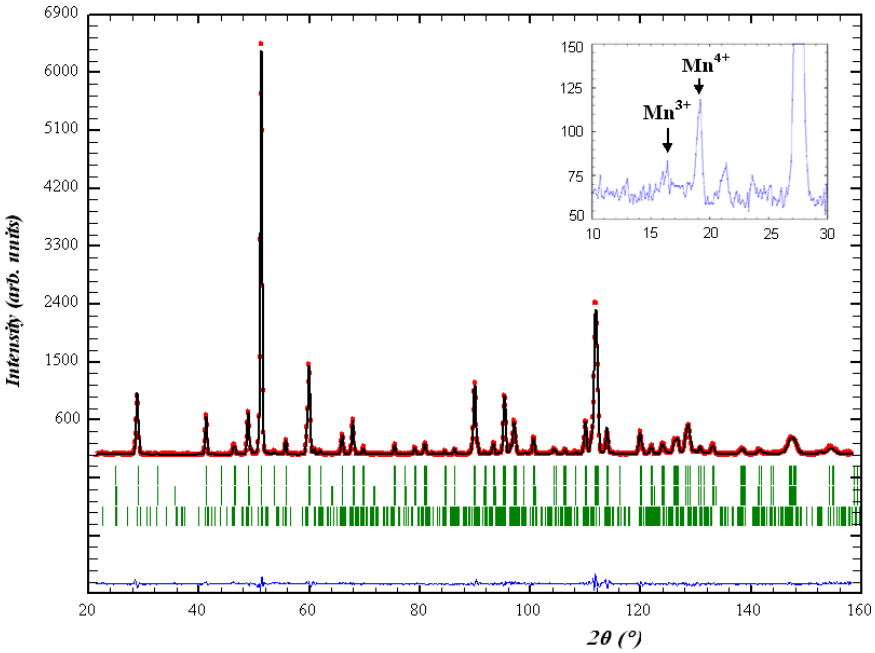

Figure 8. Rietveld refinement plot for $(La_{0.50}Ca_{0.50})(Mn_{0.97}Ni_{0.03})O_3$ (data collected at 10 K); the inset shows faint AFM peaks in the low angle region of the NPD pattern. The points in the upper field represent the observed intensity data, the calculated pattern is superposed and drawn as a solid line; the small vertical bars indicate the position of the allowed Bragg reflections for the orthorhombic nuclear (upper), FM (middle) and monoclinic nuclear (lower) phases; the difference between the observed and calculated patterns is plotted in the lower field.

for the Cr^{3+} substituted samples, despite the notable different values of the $[Mn^{3+}]/[Mn^{4+}]$ ratios.

Magnetization curves for Ni-substituted samples are reported in figure 1; Ni^{2+} substitution favours as well FM behaviour, but at much lesser extent. T_C strongly decreases with substitution (for $x = 0.03$: $T_C \sim 147$ K; for $x = 0.08$: $T_C \sim 67$ K), the magnetic transition is broadened compared to Cr-substituted samples and this broadening increases as the amount of Ni increases. In the sample with $x = 0.03$ the FM signal is dominating, but the inverse magnetization curve shows a clear deviation from the Curie–Weiss law. In the sample with $x = 0.08$ a smooth reversible increase of magnetization is observed up to ∼60 K, where a spin-glass type irreversibility between ZFC and FC curves is observed. The M–H curves measured at 5 K and up to 5.5 T for these samples do not saturate (figure 2), suggesting the occurrence of phase separation. The FM saturation moment can still be obtained by plotting magnetization as a function of the inverse of the magnetic field; in this way it is possible to separate the behaviour due to each phase [23]. The FM saturation moment can be obtained extrapolating the linear behaviour to high fields; the resulting M_s are ∼2.91 μ_B and ∼2.37 μ_B for $x = 0.03$ and 0.08, respectively. By comparison with the theoretical values the FM fractions in the samples can again be calculated.

For $(La_{0.50}Ca_{0.50})(Mn_{0.97}Ni_{0.03})O_3$ the NPD patterns exhibit a SANS behaviour similar to that observed in the Cr-substituted samples, characterized by an abrupt suppression of this contribution as the FM ordering takes place, whereas for $(La_{0.50}Ca_{0.50})(Mn_{0.92}Ni_{0.08})O_3$ an extremely faint decrease of SANS contribution can be detected comparing the NPD patterns collected at 300 and 10 K, indicating the maintenance of magnetic clusters at low T (figure 5).

A closer examination of the NPD patterns reveals that in both samples phase separation takes place on cooling; this fact is corroborated by Rietveld refinement (figure 8) revealing a notable improvement of the agreement factors in the case that the structural model foresees two different nuclear phases, the former orthorhombic (structural data are reported in tables 2 and 3), the latter monoclinic. Since that the monoclinic phase gives a small contribution to the total integrated intensities, lattice parameters only were refined, but not atomic positions and thus structural data of this phase are not reported in table 3. Figure 3 (right panel) shows a selected portion of the $(La_{0.50}Ca_{0.50})(Mn_{0.97}Ni_{0.03})O_3$ NPD patterns collected around the orthorhombic to monoclinic structural transition evidencing anisotropic line broadening towards high angle (arrowed) that is originated by the occurrence of the secondary monoclinic phase. Anyway in both substituted samples the main phase is orthorhombic. The relative amount of the monoclinic phase decreases with Ni content and the evolution of its lattice parameters with T exhibits the typical behaviour observed in charge and orbital ordered manganites (figure 9). This result indicates that the dissolved Ni^{2+} hinders the orthorhombic to monoclinic phase transition, but it is less efficient than Cr^{3+}.

In the $(La_{0.50}Ca_{0.50})(Mn_{0.97}Ni_{0.03})O_3$ NPD patterns FM peaks arise for $T \leqslant 150$ K, whose intensities progressively increase on cooling; for $(La_{0.50}Ca_{0.50})(Mn_{0.92}Ni_{0.08})O_3$ FM peaks are observed at $T \leqslant 80$ K as well. As in the case of the Cr-substituted samples, several magnetic structural models were tested in order to ascertain if the Ni^{2+} moments are magnetically aligned with those of the Mn ions: also in this case the best result in terms of *R-magnetic* factor was obtained with the structural model foreseeing a random orientation of the Ni^{2+} spins within a framework of FM aligned Mn magnetic

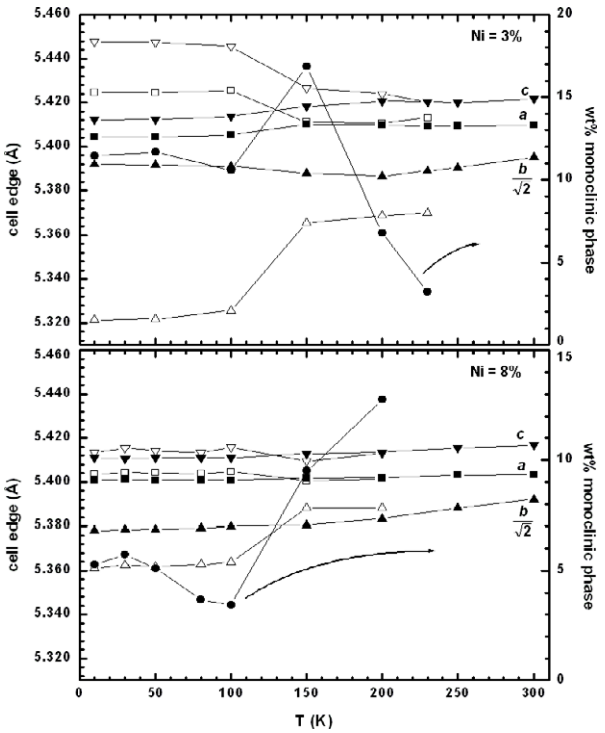

Figure 9. Evolution of the cell parameters and monoclinic phase weight percentage as a function of T for $(La_{0.50}Ca_{0.50})(Mn_{0.97}Ni_{0.03})O_3$ and $(La_{0.50}Ca_{0.50})(Mn_{0.92}Ni_{0.08})O_3$; error bars are smaller than the symbols; closed symbols refer to the orthorhombic phase, open symbols to the monoclinic phase.

moments. This result indicates that also in this case double or superexchange interactions do not take place between Ni^{2+} and the neighbouring Mn ions. The magnetic moments of Mn ions are aligned parallel to the c axis and amount to 2.96(3) μ_B and 1.12(4) μ_B for $x = 0.03$ and 0.08, respectively.

For both samples at $T \leqslant 50$ K faint AFM peaks arise, consistent with the Mn^{4+} sublattice of the *CE*-type ordering (figure 8, inset); magnetic reflections of the Mn^{3+} sublattice are hardly distinguishable from the background. In the case of the $(La_{0.50}Ca_{0.50})(Mn_{0.92}Ni_{0.08})O_3$ sample the peaks are extremely faint and broaden with the decrease of T. Undoubtedly the occurrence of these peaks is related to the presence of the monoclinic phase.

3.4. Discussion

From SANS behaviour it is evident that FM clusters are present above the magnetic transition in both the pristine and substituted samples and their formation is independent on substitution. In all samples these magnetic clusters are suppressed with the magnetic structure arising, with the exception of $(La_{0.50}Ca_{0.50})(Mn_{0.92}Ni_{0.08})O_3$. Noteworthy in the sample $(La_{0.50}Ca_{0.50})MnO_3$ the suppression of SANS does not occur around T_C, but with AFM spin ordering arising that is coupled with CO and OO. Hence it may be argued that the structural transition suppresses the magnetic clusters or, at least, reduces their volume. Conversely for the Cr-substituted samples and $(La_{0.50}Ca_{0.50})(Mn_{0.97}Ni_{0.03})O_3$, FM clusters increase in size and finally percolate on cooling; as a result a long range FM state is obtained and SANS disappears (figure 5).

In $(La_{0.50}Ca_{0.50})(Mn_{0.92}Ni_{0.08})O_3$ only a faint decrease of SANS can be appreciated from the comparison of the NPD patterns collected at 300 K and 10 K, respectively. This feature is not related to the presence of the secondary monoclinic phase; in fact the sample $(La_{0.50}Ca_{0.50})(Mn_{0.97}Ni_{0.03})O_3$ contains an higher amount of this secondary phase (figure 9), but SANS disappears at low T. Noteworthy the refined magnetic moment at 10 K is strongly lower than the theoretical one, indicating a low percentage of FM volume (∼36%). A similar feature was observed in Ga substituted $(La_{0.67}Ca_{0.33})MnO_3$ and was related to the coexistence of long range FM with short range magnetic correlations; in particular it was concluded that the substituting ion favours the localization of the e_g electrons thus hindering double exchange [24]. In our sample the situation is slightly different because the sample is located in the electron doped region of the phase diagram, but double exchange is similarly hindered to some extent on account of the low content of itinerant e_g electrons that are able to induce long range FM. Under 5.5 T the percentage of FM phase increases up to ∼76%. It has been demonstrated that the FM correlation length in these clusters increases with the magnetic field, thus increasing their size; above a critical threshold percolation takes place, producing the long range FM state [25]. Hence it may be concluded that when $(La_{0.50}Ca_{0.50})(Mn_{0.92}Ni_{0.08})O_3$ is cooled in absence of an external magnetic field the size of the magnetic clusters slightly increases with cooling and some of them percolate, but not all. As a result NPD patterns exhibit both weak FM diffraction lines and SANS at low T. With the application of an external magnetic field the increase of the magnetic clusters size is stressed and the percentage of the FM phase exhibits a net rise.

The refinement of the NPD data of our substituted samples clearly indicates that both Cr^{3+} and Ni^{2+} suppress the orthorhombic to monoclinic phase transition on cooling. In addition magnetic measurements reveals that these cationic species are not long range ordered within the magnetic structure.

Previous investigations evidenced that the substitution at the Mn site with Cr^{3+} and Ni^{2+} induces similar effects in half doped manganites [9, 26], although the development of the FM component is ascribed to different and sometimes contrasting mechanisms, assuming the occurrence of double [9–11], or superexchange interactions [12–14] between Cr^{3+} and Ni^{2+} and the neighbouring Mn cations. In any case these studies were never supported by accurate structural analyses. In particular the great ability of Cr^{3+} in favouring the FM component has been ascribed by several authors to its external electronic configuration $t_{2g}^3\ e_g^0$, the same characterizing Mn^{4+}, thus suggesting the possibility that this cationic species could participate in the double exchange. This scenario appears unlikely, since the participation of Cr^{3+} in this mechanism must imply the formation of the Jahn–Teller distorted Cr^{2+} species ($t_{2g}^3\ e_g^1$), whose ionic radius [27] strongly exceeds the average value of the B sublattice. The formation of Cr^{2+} would cause a prominent local shifting of the position of

surrounding atoms (thus inducing strong strain) as well as a notable change in the local electronic distribution. It is evident that an itinerant e_g electron is strongly favoured to hop by double exchange to an empty e_g orbital of a neighbouring Mn^{4+}, avoiding the one of Cr^{3+}. In this context it is worth to note that it has been experimentally demonstrated that Co and Ni do not participate in the double exchange [28], although they are able to favour FM similarly to Cr. In addition several investigations evidenced the possibility to destroy both OO and CO, as well as to favour FM, by substitution with some non-magnetic cationic species such as Al^{3+} [29–31], a species that does not participate in double or superexchange for sure.

The non participation of Cr^{3+} and Ni^{2+} in double or superexchange is also supported by an accurate examination of the magnetization data. In fact Salamon *et al* [32] demonstrated that colossal magnetoresistance is a Griffiths singularities; in particular they observed a sharp downturn in χ^{-1} just above T_C and on this basis identified the magnetic transition as a Griffiths singularity. It is worth to remind that Griffiths considered a percolation-like problem in a FM material, inside which a fraction of the magnetic atoms are substituted by vacancies or non-magnetic atoms [33]. In the case that all the atoms of the magnetic sublattice are FM ordered, the magnetic transition should occur at the so called Griffiths temperature (T_G), whereas the presence of vacancies or non-magnetic atoms shifts the transition to a lower temperature. Subsequent investigations [34, 35] defined the regime occurring between T_G and T_C as Griffiths phase. The Griffiths phase takes place in all our samples, whatever the composition of the B sublattice, as evidenced by the sharp downturn in χ^{-1} just above T_C (figure 1, lower panel). In $(La_{0.50}Ca_{0.50})MnO_3$ its occurrence can be related to the competition between double exchange and the electron–phonon coupling. A similar downturn is observed in the χ^{-1} curves of the substituted samples, thus indicating that Cr^{3+} and Ni^{2+} do not directly favour one of the two competing phenomena and as a consequence they both do not induce or participate in magnetic exchange mechanisms. Conversely in the substituted samples T_C decreases as foreseen by the Griffiths model in the case that a fraction of non-magnetic atoms is present in the magnetic lattice. This is a further clear indication that both Cr^{3+} and Ni^{2+} do not participate in magnetic exchanges.

NPD analysis reveals that both Cr^{3+} and Ni^{2+} substitution at the Mn site hinders the formation of the monoclinic phase on cooling and this is the key role played by these cationic species. In fact the suppression of the orthorhombic to monoclinic phase transition during cooling prevents both charge and orbital orderings at the Mn sublattice. As a result superexchange interactions do not occur, whereas double exchange among Mn cationic species can take place and thus their spins order FM.

Nevertheless Cr^{3+} exhibits a greater effectiveness in favouring FM, as proved by higher T_C and higher saturation moment, since in the Cr-substituted samples the monoclinic phase is completely suppressed, whereas in the Ni-substituted ones a certain amount of this phase is still present. The presence of the secondary phase in the Ni-substituted samples cannot be ascribed to a different $[Mn^{3+}]/[Mn^{4+}]$ ratio; in fact this is about the same for the sample with 3% of Ni and the one with 8% of Cr, but in the former about 10 vol% is constituted of monoclinic phase at 10 K, whereas the latter is orthorhombic as a whole. On the other hand the structural properties of the orthorhombic phase in the substituted samples are very similar: at 10 K the average Mn–O bond lengths and Mn–O–Mn bond angles are nearly the same (table 3). Since magnetic interactions are strongly dependent on these structural properties and that both substituting cationic species do not participate in double exchange, the different behaviour characterizing the Ni- and Cr-substituted samples could be related to their capability to induce particular local effects.

First of all we note that substitution at the B site reduces the $[Mn^{3+}]/[Mn^{4+}]$ ratio: in fact both Cr^{3+} and Ni^{2+} substitute Mn^{3+} decreasing its content, but in addition the dissolution of Ni^{2+} must be compensated also by the oxidation of an equivalent number of Mn^{3+} cationic species to Mn^{4+} for maintaining charge balance. This is evident when the $[Mn^{3+}]/[Mn^{4+}]$ ratios are compared in the different samples: the samples with 8% of Cr^{3+} and 3% of Ni^{2+} are characterized by almost the same value (0.84 and 0.83, respectively), whereas in the sample with 8% of Ni^{2+} this ratio is dramatically decreased (0.59). Figure 10 exemplifies this situation: a square array of 25 points is drawn and each point represents a B site of the manganite; the array on the left is a schematic representation of the charge ordered state in $(La_{0.50}Ca_{0.50})MnO_3$. For simplicity we have considered a 4% level of substitution (1 substituting cation in the 5×5 array) instead of our experimental situation. When 4% and 8% of Cr^{3+} or Ni^{2+} substitutes Mn^{3+}, magnetic interactions are suppressed in 4 and 8 B–O–Mn units, respectively (full lines in figure 10). In the case of Ni^{2+} substitution the increase of Mn^{4+} cationic species content leads also to the formation of Mn^{4+}–O–Mn^{4+} units where double exchange cannot take place (dashed lines in figure 10) and is thus contrasted. It is worth to note that the Mn^{4+}–O–Mn^{4+} units are characterized by a certain degree of itinerancy due to the itinerant character of the e_g electrons, whereas the Cr^{3+}–O–Mn and Ni^{2+}–O–Mn are localized. On this basis it is easy to understand why Cr^{3+} exhibits a greater ability in favouring FM.

In the sample $(La_{0.50}Ca_{0.50})(Mn_{0.92}Ni_{0.08})O_3$ the content of itinerant e_g electrons is dramatically decreased and is not sufficient to convert the whole mass of the sample into the FM state at ZF. On the other hand, due to the presence of itinerant e_g electrons charge ordering is hindered and hence superexchange interactions in the Mn^{4+}–O–Mn^{4+} units cannot take place; as a result a spin-glass state arises.

4. Conclusions

In conclusion we have demonstrated that Ni^{2+} and Cr^{3+} induce similar structural and magnetic modifications in $(La_{0.50}Ca_{0.50})MnO_3$, even though these ions are characterized by different external electronic configurations. Both Ni^{2+} and Cr^{3+} substitution hinders the orthorhombic to monoclinic phase transition occurring in $(La_{0.50}Ca_{0.50})MnO_3$ on cooling; as a result both charge and orbital ordering is suppressed

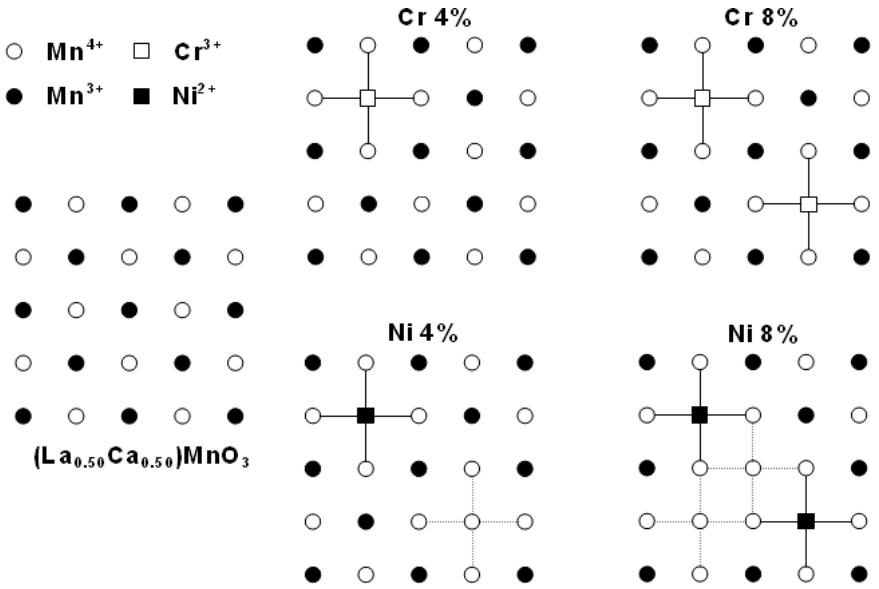

Figure 10. Effect of Cr^{3+} and Ni^{2+} substitution at the B sublattice on the exchange interactions: full lines represents B–O–Mn units where magnetic interactions are suppressed, whereas dashed lines Mn^{4+}–O–Mn^{4+} units where double exchange is prevented.

and superexchange-AFM interactions as well. Cr^{3+} is more effective than Ni^{2+}, since in the Ni-substituted samples a small amount of monoclinic AFM phase can be detected at low T. As a result of the stabilization of the orthorhombic-charge disordered phase at low T, double exchange takes place and FM interactions occur. Both Ni^{2+} and Cr^{3+} do not participate in the double exchange, thus hindering to some extent the upcome of FM, the former being more effective from this point of view. For large Ni substitution a spin-cluster glass-like state is observed.

References

[1] Raveau B and Rao C N R 2001 *Magnetism: Molecules to Materials* ed J S Miller and M Drillon (Weinheim: Wiley–VCH) pp 297–324
[2] Moreo A, Yunoki S and Dagotto E 1999 *Science* **283** 2034
[3] Chen C H and Cheong S-W 1996 *Phys. Rev. Lett.* **76** 4042
[4] Mori S, Chen C H and Cheong S-W 1998 *Phys. Rev. Lett.* **81** 3972
[5] Radaelli P G, Cox D E, Marezio M and Cheong S-W 1997 *Phys. Rev.* B **55** 3015
[6] Huang Q, Lynn J W, Erwin R W, Santoro A, Dender D C, Smolyaninova V N, Ghosh K and Greene R L 2000 *Phys. Rev.* B **61** 8895
[7] Levy P, Parisi F, Polla G, Vega D, Leyva G, Lanza H, Freitas R S and Ghivelder L 2000 *Phys. Rev.* B **62** 6437
[8] Freitas R S, Ghivelder L, Levy P and Parisi F 2002 *Phys. Rev.* B **65** 104403
[9] Maignan A, Damay F, Martin C and Raveau B 1997 *Mater. Res. Bull.* **32** 965
[10] Martin C, Maignan A, Damay F, Hervieu M, Raveau B, Jirak Z, André G and Bourée F 1999 *J. Magn. Magn. Mater.* **202** 11
[11] Sun Y, Tong W, Xu X and Zhang Y 2001 *Phys. Rev.* B **63** 174438
[12] Mahendiran R, Hervieu M, Maignan A, Martin C and Raveau B 2000 *Solid State Commun.* **114** 429
[13] Cabeza O, Long M, Severac C, Bari M A, Muirhead C M, Francesconi M G and Greaves C 1999 *J. Phys.: Condens. Matter* **11** 2569
[14] Gundakaram R, Arulraj A, Vanitha P V, Rao C N R, Gayathri N, Raychaudhuri A K and Cheetham A K 1996 *J. Solid State Chem.* **127** 354
[15] Rodríguez-Carvajal J 1993 *Physica* B **192** 55
[16] Goodenough J B 1955 *Phys. Rev.* **100** 564
[17] Bertaut E F 1968 *Acta Crystallogr.* A **24** 217
[18] Damay F, Martin C, Maignan A, Hervieu M and Raveau B 1998 *Appl. Phys. Lett.* **73** 3772
[19] Frontera C, García-Muñoz J L, Llobet A, Ritter C, Alonso J A and Rodríguez-Carvajal J 2000 *Phys. Rev.* B **62** 3002
[20] Rodriguez E E, Proffen Th, Llobet A, Rhyne J J and Mitchell J F 2005 *Phys. Rev.* B **71** 104430
[21] Martinelli A, Ferretti M, Castellano C, Mondelli C, Cimberle M R, Tropeano M and Ritter C 2006 *Phys. Rev.* B **73** 064423
[22] De Teresa J M, Ibarra M R, Blasco J, García J, Marquina C, Algarabel P A, Arnold Z, Kamenev K, Ritter C and von Helmolt R 1996 *Phys. Rev.* B **54** 1187
[23] Levy P, Parisi F, Polla G, Vega D, Leyva G, Lanza H, Freitas R S and Ghivelder L 2000 *Phys. Rev.* B **62** 6437
[24] De Teresa J M, Algarabel P A, Ritter C, Blasco J, Ibarra M R, Morellon L, Espeso J I and Gómez-Sal J C 2005 *Phys. Rev. Lett.* **94** 207205
[25] De Teresa J M, Algarabel P, Ibarra M R, Morellon B, García-Landa B, Marquina C, Ritter C, Maignan A, Martin C, Raveau B, Kurbakov A and Trounov V 2002 *Phys. Rev.* B **65** 100403
[26] Barnabé A, Maignan A, Hervieu M and Raveau B 1998 *Eur. Phys. J.* B **1** 145
[27] Shannon R D 1976 *Acta Crystallogr.* A **32** 751
[28] Rubinstein M, Gillespie D J, Snyder J E and Tritt T M 1997 *Phys. Rev.* B **56** 5412
[29] Takenaka K, Okuyama S, Shiozaki R, Fujita T and Sugai S 2002 *J. Appl. Phys.* **91** 2994
[30] Damay F, Maignan A, Martin C and Raveau B 1997 *J. Appl. Phys.* **82** 1485
[31] Banerjee A, Mukherjee K, Kumar K and Chaddah P 2006 *Phys. Rev.* B **74** 224445
[32] Salamon M B, Lin P and Chun S H 2002 *Phys. Rev. Lett.* **88** 197203
[33] Griffiths R B 1969 *Phys. Rev. Lett.* **23** 17
[34] Bray A J and Moore M A 1982 *J. Phys. C: Solid State Phys.* **15** L765
[35] Bray A J 1987 *Phys. Rev. Lett.* **59** 586